Numerical modeling on vibroflotation soil improvement techniques using a densification constitutive law

Article *in* Soil Dynamics and Earthquake Engineering · October 2014

Impact Factor: 1.22 · DOI: 10.1016/j.soildyn.2014.05.010

3 authors:

Susana López-Querol
University College London
34 PUBLICATIONS **87** CITATIONS
SEE PROFILE

Jaime Peco
Spanish National Research Council
6 PUBLICATIONS **8** CITATIONS
SEE PROFILE

Juana Arias-Trujillo
Universidad de Extremadura
8 PUBLICATIONS **13** CITATIONS
SEE PROFILE

Soil Dynamics and Earthquake Engineering 65 (2014) 1–10

Contents lists available at ScienceDirect

Soil Dynamics and Earthquake Engineering

journal homepage: www.elsevier.com/locate/soildyn

Numerical modeling on vibroflotation soil improvement techniques using a densification constitutive law

Susana López-Querol [a,*], Jaime Peco [b,1], Juana Arias-Trujillo [c,2]

[a] School of Computing and Technology, University of West London, Villiers House, W5 2NU London, UK
[b] Department of Civil Engineering, University of Castilla - La Mancha, Avda. Camilo Jose Cela s/n, 13071 Ciudad Real, Spain
[c] School of Engineering, Department of Construction, University of Extremadura, Avda. de la Universidad s/n, 10003 Cáceres, Spain

ARTICLE INFO

Article history:
Received 13 May 2013
Received in revised form
11 May 2014
Accepted 25 May 2014

Keywords:
Densification
Soil improvement techniques
Finite element modeling
Absorbing boundary conditions
Vibroflotation

ABSTRACT

The densification phenomenon in dry or completely drained sands mainly occurs when these materials are subjected to dynamic loadings. This fact induces a reduction of voids volume and consequently the compaction of the soil. The Generalized Endochronic densification law, formulated in cylindrical coordinates, has been used in a finite element model for simulating vibroflotation soil improvement techniques. The effects of vibrations at a point inside the soil mass, like those applied in vibroflotation treatment, are reproduced with this code. Absorbing boundary conditions are established at those borders where spatial domain finishes, aiming to avoid spurious, artificial reflections of stress waves, which otherwise come into the domain, disturbing the computed results. A mean densification function is defined for each spatial domain, to evaluate the effect of this technique, and also employed to optimize the distance between vibration points. This is a new rational design approach, which represents a step forward development if it is compared with the usual empirical employed procedures.

1. Introduction

Vibroflotation is a technique for improving the strength and bearing capacity of unsaturated, granular soils. This technique consists of the application of punctual vibrations at different depths inside a soil layer, produced by a device called “vibrator”. These vibrations can have different amplitudes and frequencies, causing dynamic loadings inside the soil (Fig. 1). This soil improvement technique was first used in Germany in the 1930s, and later, in USA. It is specially recommended for soils with very small fines content and for deep layers, taking into account that the vibrator can be introduced within the soil until 20 m, approximately. For a given soil and vibrator, with its particular amplitude and frequency of loading, this procedure requires the definition of several geometrical parameters, i.e. the vertical distance between vibrating points at the same hole, as well as the horizontal distance between them, or the time of vibration at each location. In practice, these magnitudes are usually defined by means of empirical approaches, trials before the complete treatment, and by using data derived from successful past experiences. Although this technique has been successfully applied in many cases [1,2], it seems to be necessary the development of a rational design approach.

It is well known that, when loose sandy soils are subjected to dynamic loadings, they tend to acquire denser states, reorganizing their grains. This phenomenon is known as densification.

To model this kind of processes, several approaches can be adopted. On one hand, there are empirical and semi-empirical based models, which extrapolate the results of densification found in laboratory for a particular material. These models usually give good results, but they are far from reproducing the physical mechanisms governing the real soil behavior [3–5].

On the other hand, it is possible to find in the literature other different cases aiming to model that phenomena in granular soils. Bement and Selby [6] studied experimentally the problem of soil densification during pile driving and emphasized the role of stress level and granulometric properties of the soil to be treated. Arnold and Herle [7] developed a numerical model to simulate the soil densification obtained throughout the vibrocompaction technique, comparing deep and top vibrators. Their model was based on a mix of dynamic FE calculation at first, to obtain strain paths, and hypoplasticity theory [8,9] with intergranular strains applied to the soil to be improved in the second step. This model required a huge computational time since a 3D FE approach was employed, and the agreement between numerical simulations and field data was not good. Finally, other models like generalized plasticity have not still been widely tested in vibroflotation models for granular

* Corresponding author. Tel.: +44 2082312127.
E-mail addresses: susana.lopez-querol@uwl.ac.uk (S. López-Querol), jaime.peco@gmail.com (J. Peco), jariastr@unex.es (J. Arias-Trujillo).
[1] Tel.: +34 926295300x6237.
[2] Tel.: +34 927257000x51620.

http://dx.doi.org/10.1016/j.soildyn.2014.05.010
0267-7261/

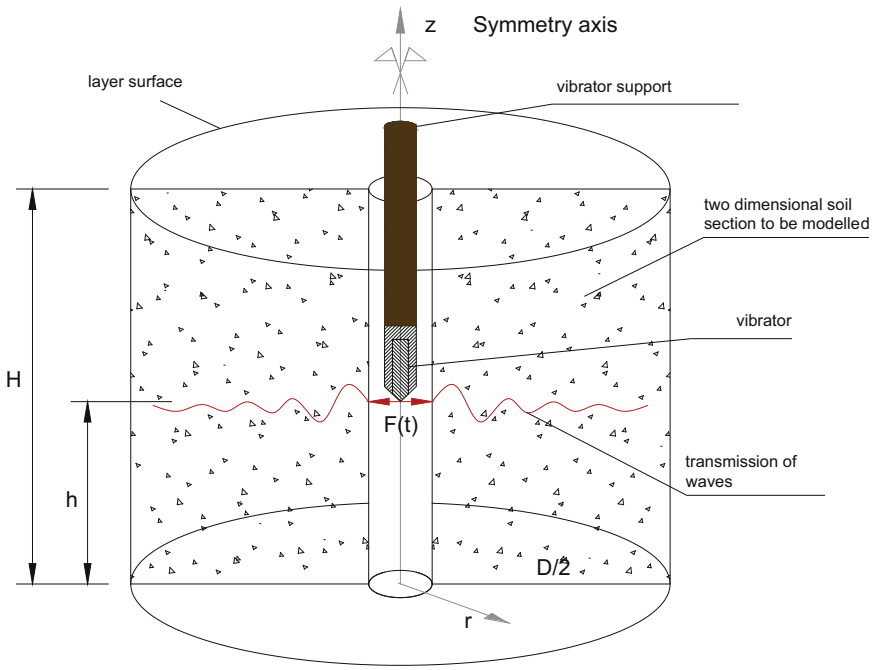

Fig. 1. Sketch of the vibroflotation soil improvement technique. Details of a hole, including the vibrator inside.

soils, and their feasibility for this kind of problems is still to be explored.

In this research, an endochronic based densification law for sandy material is used. The Endochronic Theory, first developed for metals, was successfully applied to sandy materials subjected to vibrations by Cuéllar [10,11]. This law, based on the definition of two monotonic functions which increase as the number of harmonic shear strain cycles progresses, has been recently updated and generalized for non-harmonic loadings and high number of cycles [12].

The above-mentioned endochronic based densification law has been implemented in a Finite Element code, formulated for axi-symmetric problems. In this paper, a single hole and its surrounding soil have been modeled. The axis of symmetry has been placed in the hole, where punctual vibrations could take place at different depths. Aiming to avoid the unrealistic reflection of stress waves into the domain of interest, absorbing boundary conditions have been established at those boundaries which mark the limits of the numerical domain but are surrounded by soil in real field situations.

At the beginning, the paper shows the particularities of the numerical model, including the employed constitutive law, the axi-symmetrical formulation of FE code, as well as the implementation of absorbing boundary conditions. After that, the model is applied to different materials and the optimal spacing of the vibration points is established.

2. Description of the numerical model

2.1. Constitutive law

In his pioneer work, Cuéllar (1974) established that the densification of sand is due to the irreversible rearrangement of grain configurations associated to the application of a deviatoric strain. In mathematical form:

$$d\xi = f(d\varepsilon_{ij}) \tag{1}$$

where ξ is called *rearrangement measure*, which is a function of the deviatoric component of the strain tensor, ε_{ij}. In order to account for the monotonically increasing trend of ξ, the differential expression given by Eq. (2) must be a quadratic and finite function:

$$d\xi = (P_{ijkl} \cdot d\varepsilon_{ij} \cdot d\varepsilon_{kl})^{1/2} \tag{2}$$

where P_{ijkl} denotes a tensor, the components of which are material state dependent.

Neglecting the dependence of $d\xi$ on the third invariant of the increment of strains tensor, it is hence possible to uncouple Eq. (2) as follows:

$$d\xi = [P_1 \cdot I_1^2(d\varepsilon_{ij}) + P_2 \cdot J_2^2(d\varepsilon_{ij})]^{1/2} \tag{3}$$

where $I_1(\ldots)$ and $J_2(\ldots)$ respectively represent the first and second invariant of the tensor between brackets, and P_1 and P_2 are model parameters. It is demonstrated that dynamic volumetric strains cause a small effect on the amount of densification [13], so the term $I_1^2(d\varepsilon_{ij})$ can be neglected in Eq. (3), yielding:

$$d\xi = [P_2 \cdot J_2^2(d\varepsilon_{ij})]^{1/2} \tag{4}$$

Moreover, a monotonic function ζ, called *densification measure*, is also defined, and like ξ is time independent. This function depends on ξ, and is incrementally defined:

$$d\zeta = F_1(J_2(d\varepsilon_{ij})) \cdot d\xi \tag{5}$$

where F_1 denotes an analytical function, and $d\varepsilon_{ij}$ represents the increment of the strain tensor.

Finally, the densification ε_y' (volumetric strain) is incrementally defined as follows:

$$d\varepsilon_y' = -F_2(\zeta, Dr_0) \cdot d\zeta \tag{6}$$

where F_2 is a function, and Dr_0 is the initial relative density of the sand before it is subjected to dynamic loading. Cuéllar [10] proposed the next expressions for F_1 and F_2:

$$F_1 = \frac{n}{4} \cdot |100 \cdot \gamma|^{n-1} \tag{7}$$

$$F_2 = \frac{1}{1+\alpha \cdot \zeta} \tag{8}$$

where n and α are parameters and γ denotes the shear strain expressed in per one.

The densification law proposed by Zienkiewicz et al. [14] is based in a very similar approach, with an almost identical expression for F_2, but with an exponential function for F_1.

In the particular case of quartzitic sands, Blázquez and López-Querol [12] demonstrate that n and α can only be assumed as constant for a low number of cycles of loading. They also found a relationship between both parameters and the number of cycles of harmonic shear strain, N:

$$n = A \cdot \ln(N) + B \tag{9}$$

$$\alpha = C \cdot N^{-D} \tag{10}$$

where A, B, C and D are model parameters, which depend on initial relative density, maximum and minimum voids ratio. The proposed final expressions for these parameters are

$$A = \frac{1}{2} \cdot \left[\frac{e_{max}^2 - e_{min}^2}{1 + e_{max} - Dr_0 \cdot (e_{max} - e_{min})} \right] \tag{11}$$

$$B = 1 + \tfrac{1}{2} \cdot (e_{max}^2 - e_{min}^2) \tag{12}$$

$$D = \tfrac{1}{2} \cdot (e_{max}^2 - e_{min}^2) \tag{13}$$

C is the only remaining coefficient, initial relative density dependent, which needs to be calibrated by means of dynamic tests.

For a given sand, this approach allows generalizing the densification law for different initial densities and confining stresses.

For the whole definition of the problem, a stress–strain correlation is also required. The law for variation of the elastic modulus proposed by [15] is employed herein. According to this law, the elastic shear modulus, G, varies as follows:

$$G = \frac{G_0}{T} \tag{14}$$

where G_0 denotes the initial elastic shear modulus and is calculated as

$$G_0 = \frac{B_g \cdot p_a}{0.3 + 0.7 \cdot e^2} \cdot \left(\frac{p'}{p_a} \right)^{0.5} \tag{15}$$

B_g is a sand dependent model parameter, e is the voids ratio, p' represents the effective confining stress, and p_a is the atmospheric pressure.

In Eq. (14), T denotes the degradation parameter, which for the first loading is computed as

$$T = 1 + 2 \cdot C_t |\eta - \eta_0| \tag{16}$$

and for unloading and reloading, is obtained with:

$$T = 1 + C_t |\eta - \eta_{sr}| \tag{17}$$

In the above expressions, C_t is a model parameter, depending on the degree of non-linearity of the soil response, and η, η_0 and η_{sr} represent current, initial and last reversal values of τ/σ'_v respectively.

Several investigations [12,16,17] have demonstrated this law that works with fair accuracy not only for dry, but also for saturated, quartzitic, sandy materials.

2.2. Finite Element code

The geometry of the problem consists of a vibrating point placed within the soil mass. Figs. 1 and 2 represent the scheme of the treatment for a single point. From the inspection of these figures, the axi-symmetrical nature of the problem is self-evident. Hence, a Finite Element code, formulating the equilibrium equations in axi-symmetric coordinates, has been developed [18], only valid when the soil properties are independent of the circular coordinate, θ. Coordinate z represents the depth measure from the surface, and r denotes the horizontal distance to the vertical line occupied by the vibrator (axis), as shown in Fig. 3.

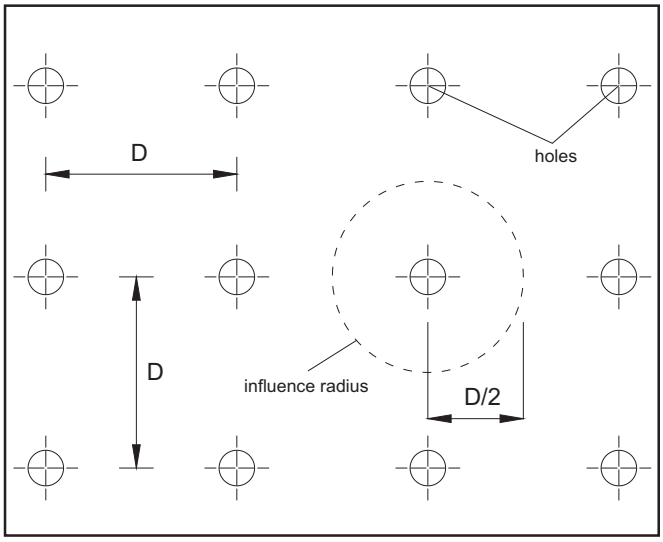

Fig. 2. A plant view of the mesh of holes in the soil layer to be improved.

In such axi-symmetrical problems, the weak formulation of the governing equation, in its incrementally form, and without taking into account damping terms, is given by

$$\int_\Omega \left[\frac{\partial N_i}{\partial l} [D]^e \frac{\partial N_j}{\partial m} \right] \cdot \{\Delta d\} \, d\Omega + \int_\Omega [N_i \rho N_j] \cdot \{\Delta a\} \, d\Omega = \int_\Omega [N_i \rho] \cdot \{\Delta a_g\} \, d\Omega + \{\Delta f_{ext}\} \tag{18}$$

where Ω denotes the spatial domain, N are shape functions, $\{\Delta d\}$ and $\{\Delta a\}$ are the incremental displacement and acceleration vectors respectively, ρ represents the soil density, $[D]^e$ is the elastic constitutive law tensor (formulated according to the reference coordinates system $r-z$), and $\{\Delta a_g\}$ is the vector of incremental gravitational accelerations. The above equation finally yields

$$[\mathbf{K}] \cdot \{\Delta d\} + [\mathbf{M}] \cdot \{\Delta a\} = \{\Delta f_g\} + \{\Delta f_{ext}\} \tag{19}$$

where $[\mathbf{K}]$ and $[\mathbf{M}]$ respectively represent stiffness and mass matrices, and $\{\Delta f_{ext}\}$ is the incremental external force vector, where the punctual vibration at a node (vibrating point) is implemented. ∂l, ∂m are ∂r, ∂z, and $\{\Delta f_g\}$ is the incremental body forces vector.

In Appendix A, details on shape functions, matrix elementary components and assembling, are given.

To solve the problem in the time domain, the implicit step-by-step Newmark's time integration scheme ($\beta_1 = \beta_2 = 0.5$) [19,20] has been implemented in the code.

2.3. Absorbing boundary conditions

2.3.1. Description and formulation

The problem analyzed in this research is based on the transmission of seismic waves through the soil mass, caused by punctual vibrations. These waves produce the accumulation of shear strains to occur, and hence, volumetric strains (densification), according to the constitutive law described in Section 2.1. If usual boundary conditions (preventing displacements) were applied at the space domain limits, when the seismic waves arrive to them, they would be reflected into the spatial domain introducing artificial vibrations, since in a real field case this wave reflection does not happen. This spurious reflections reintroduced into the domain could affect the solution in a very strong way, even invalidating it, if they reach the area or points of interest. Hence, for sake of accuracy, it is necessary to establish absorbing boundaries, where reflection is not allowed, and at the same time, to allow the

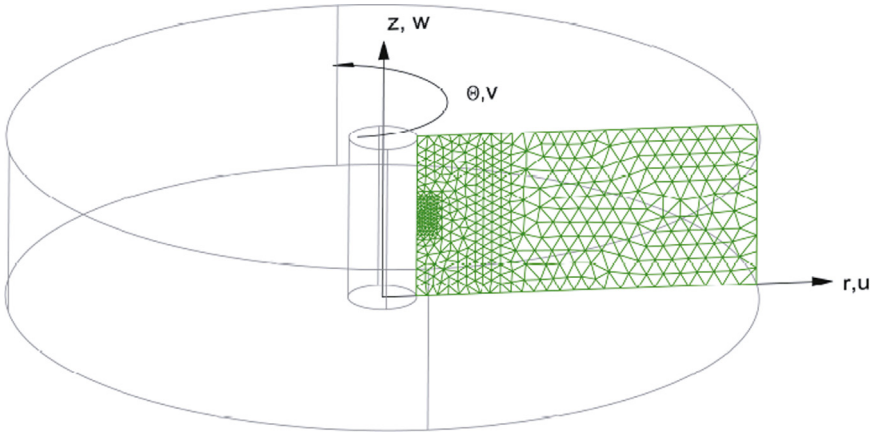

Fig. 3. Axisymmetric FE model for vibroflotation.

waves leaving the spatial domain. On the other side, when absorbing boundaries are implemented, a reduction in the size domain can be adopted, supposing an improvement from a computational cost point of view.

In this research, the absorbing boundaries developed by Lysmer and Kuhlemeyer [21], based on viscous damping forces, have been implemented following the approach presented by Toshinawa and Ohmachi [22]. Thus, the dissipation of a vibrational wave is simulated at those borders where it arrives. A damping matrix [**C**], is included into the general governing equation (19), yielding the next final expression:

$$[\mathbf{K}]\cdot\{\Delta d\}+[\mathbf{C}]\cdot\{\Delta v\}+[\mathbf{M}]\cdot\{\Delta a\}=\{\Delta f_g\}+\{\Delta f_{ext}\} \tag{20}$$

In this particular problem, without initial damping matrix [**C**], its only no null components are those correspondent to the nodes located at the silent boundaries. If an initial damping matrix already exists before applying absorbing boundaries, these new damping components at the absorbing nodes, are summed to the previous correspondent values at matrix [**C**].

Toshinawa and Ohmachi [22] exposed a formulation for 3D, linear approximation FE problems. The required simplifications for 2D axi-symmetrical problem, with triangular elements and quadratic approximation, are employed hereinafter. In such a case, the element damping matrix, $[\mathbf{C}]^e$, is square and 12×12 size, and all of them must be assembled to obtain [**C**].

The element damping matrix, $[\mathbf{C}]^e$, changes depending on the side of the element located at the absorbing boundary (or, in other words, on the three nodes placed on that absorbing border, if quadratic approximation is considered). In Fig. 4, the labels of these nodes are depicted. As an example, if the side defined by nodes *i*, *l* and *j* (local numbers: 1, 4 and 2, respectively) defines the silent boundary, the corresponding element damping matrix, $[\mathbf{C}]^e$, must be determined as follows:

$$[\mathbf{C}]^e=\frac{\rho L_{12}}{4}\begin{pmatrix} V_X & 0 & 0 & 0 & 0 & 0 & 0 & 0 & 0 & 0 & 0 & 0\\ & V_Y & 0 & 0 & 0 & 0 & 0 & 0 & 0 & 0 & 0 & 0\\ & & V_X & 0 & 0 & 0 & 0 & 0 & 0 & 0 & 0 & 0\\ & & & V_Y & 0 & 0 & 0 & 0 & 0 & 0 & 0 & 0\\ & & & & 0 & 0 & 0 & 0 & 0 & 0 & 0 & 0\\ & & & & & 0 & 0 & 0 & 0 & 0 & 0 & 0\\ & & & & & & 2\cdot V_X & 0 & 0 & 0 & 0 & 0\\ & & & & & & & 2\cdot V_Y & 0 & 0 & 0 & 0\\ & & Sim. & & & & & & 0 & 0 & 0 & 0\\ & & & & & & & & & 0 & 0 & 0\\ & & & & & & & & & & 0 & 0\\ & & & & & & & & & & & 0 \end{pmatrix} \tag{21}$$

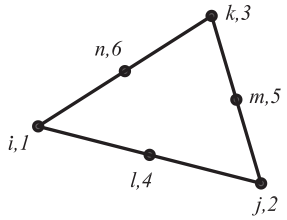

Fig. 4. Quadratic, triangular finite element: local labels of its six nodes.

where ρ denotes soil density, L_{ij} represents the length of the element side on the silent boundary defined between nodes *i* and *j*, $V_X=v_s\cos(\theta_X)+v_c\sin(\theta_X)$, $V_Y=v_s\cos(\theta_Y)+v_c\sin(\theta_Y)$, where θ_X is the angle between the silent boundary and the horizontal axis, and θ_Y, the angle between the silent boundary and the vertical axis. v_c and v_s are waves velocities, defined next:

$$v_c=\sqrt{\frac{D}{\rho}} \tag{22}$$

$$v_s=\sqrt{\frac{G}{\rho}} \tag{23}$$

where *D* and *G* are constrained and shear elastic moduli, respectively.

2.3.2. Validation example

For validating the above described methodology, an infinite elastic soil column subjected to a vertical force on its surface, *p*, has been adopted, Fig. 5. The vertical displacement suffered by a point placed 1 m below the soil surface in a column 5 m deep is analyzed. This displacement is obtained both with and without silent boundary at the bottom of the column, and compared to the analytical solution for the infinite column proposed by [23]:

$$w(z,t)=\frac{p\cdot v_c\cdot(t-z/v_c)}{E}\cdot H(t-z/v_c) \tag{24}$$

where *w* denotes vertical displacement, *z* is the depth (from the surface) where the vertical displacement is to be obtained, *E* represents the elastic modulus, $H(\cdots)$ represents the Heaviside function, and *t* is the time from the application of the loading. If the silent boundary is working properly, almost identical vertical displacements are expected to be obtained when analytical solution and numerical result (including silent boundary) are

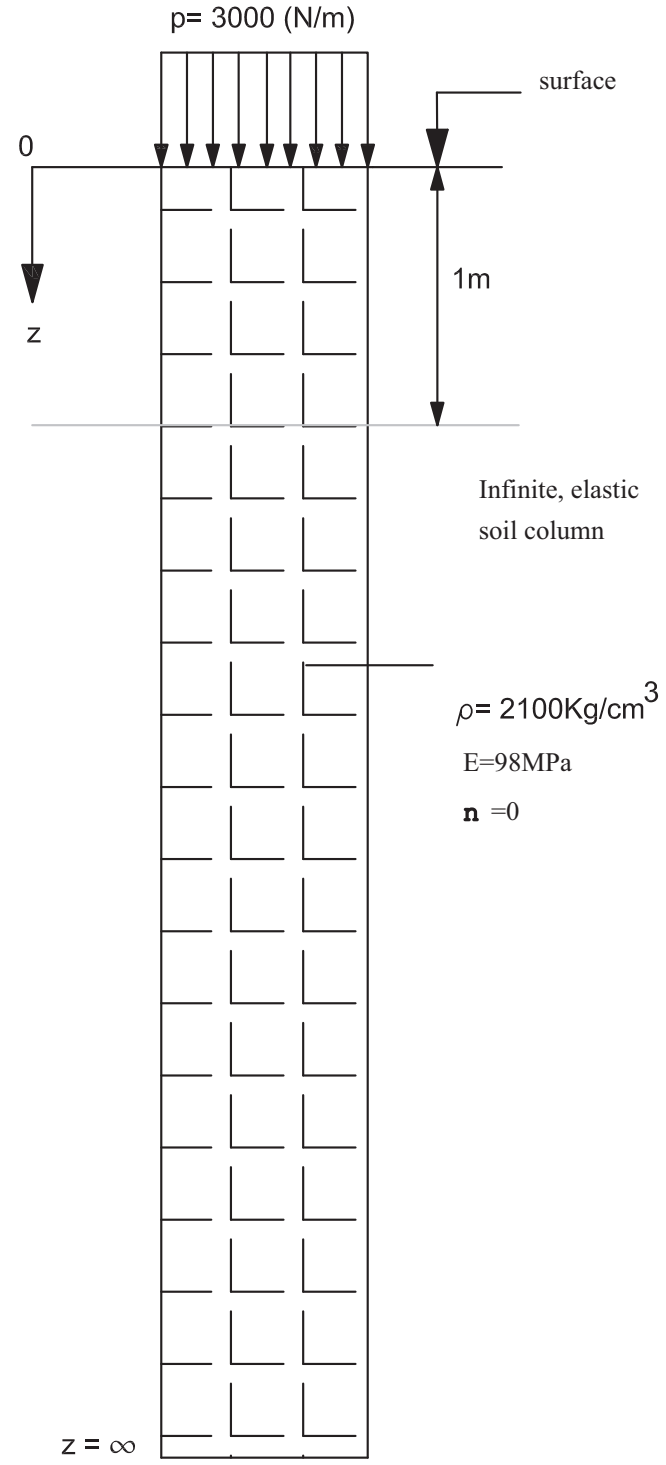

Fig. 5. Infinite elastic soil column subjected to vertical loading.

compared. Fig. 6 shows that comparison and addresses the accuracy of the employed formulation.

The same approach has been formulated in $r-z$ coordinates and implemented in the code for modeling vibroflotation processes. For that problem, the absorbing boundaries are the lateral ones, which are not rigid boundaries in the field, since they are surrounded by soil, letting the waves to pass through them and leaving the spatial domain.

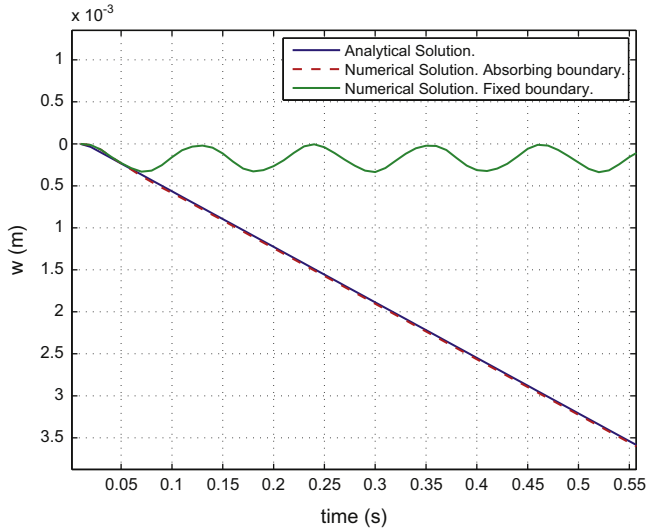

Fig. 6. Vertical displacement 1 m below the soil surface for an infinite column: comparison between exact and numerical solutions, with and without silent boundary.

3. Computation of the densification produced by vibroflotation treatment

3.1. General features

The densification produced by vibroflotation treatment in granular soils is obtained by means of the above described numerical tool. The computational procedure is based on an uncoupled elastic-plastic approach: the governing equations in the FE scheme include the constitutive elastic tensor D^e, the properties of which are updated step-by-step, as a result of the application of the constitutive model of densification described in Section 2.1. At the end of this calculation, unrecoverable volumetric strains, as the consequence of the dynamic process, are obtained. The time domain is divided in equal increments of time Δt. For each step of calculation, the next stages are followed:

1. Beginning of the calculation at time t.
2. Computation of stiffness and mass matrices, [**K**] and [**M**], as well as damping matrix due to absorbing boundaries, [**C**].
3. Calculation of increment of external force vector, $\{\Delta f_{ext}\}$, which includes the effect of the vibrator at the point of vibration.
4. By means of Newmark's time integration scheme, incremental nodal displacement, velocity and acceleration vectors, $\{\Delta d\}$, $\{\Delta v\}$ and $\{\Delta a\}$ are obtained at the current time step.
5. Strains and stresses are calculated by means of the current soil properties.
6. Using the current stresses and strains obtained in the previous stage, the increment of densification is computed at each element.
7. Voids ratio, e, and shear elastic modulus, G, are updated through the increment of densification previously obtained. These new values will be used to update matrices [**K**], [**M**] and [**C**] in the next time step.
8. The computation at the current time step is finished. The new step at time $t+\Delta t$ is ready to begin.

The variables which must be defined in the model, according to Fig. 1, are

- D: distance between neighbor holes (Fig. 2).
- H: layer depth.

- h: elevation of the vibrating point, measured from the bottom of the soil layer.
- t: time of vibration at each point.
- f: vibration frequency (in Hz) applied by the vibrator.
- F_{max}: amplitude of vibration (horizontal force).
- Dr_0: initial relative density of the soil to be improved.

One of the most important issues in a vibration procedure is to optimize the mean densification at the spatial domain for the minimum possible time of treatment. As a result, the optimal distance between points of vibration will be determined.

3.2. Definition of mean densification function

At a given spatial domain, the mean densification function, ϕ_y, is defined as follows:

$$\phi_y = \frac{\sum_{i=1}^{i=N_e}(A_i \cdot \varepsilon'_{y_i})}{\sum_{i=1}^{i=N_e} A_i} = \frac{\sum_{i=1}^{i=N_e}(A_i \cdot \varepsilon'_{y_i})}{A_{TOTAL}} \tag{25}$$

where A_i and ε'_{y_i} respectively denote area and densification at element i, and N_e is the total number of elements in the domain.

3.3. Characteristics of the applied vibration

The rotation of the engine into the vibrator causes a harmonic, horizontal vibration at the point of application within the soil mass. The amplitude of this displacement is given by the features of each device. In the above described numerical model, a horizontal, harmonic force is applied at the point of vibration. This force is

$$F(t) = F_{max}\ \sin(2\pi f t) \tag{26}$$

A conventional vibrator KELLER L-BETA, the properties of which are summarized in [24], has been used. These features are defined in Table 1. In addition, the time of vibration at each point has been fixed as $t = 10$ s, and hence, 600 cycles are applied (since its frequency is 60 Hz). As it is common, the time step has been chosen equal to $T_{cycle}/20$, this is equivalent to tenth of the maximum possible time step according to Nyquist's criterion. This value guarantees that aliasing phenomena will be avoided and at the same time, accurate enough results will be achieved [25]. Hence, the time step Δt is equal to:

$$\Delta t = \frac{1}{20 \cdot f\ (\mathrm{Hz})} = 8.3 \times 10^{-4}\ \mathrm{s}. \tag{27}$$

Additionally, a force amplitude $F_{max} = 50$ kN has been tested, producing required horizontal amplitude of displacement equal to 5 mm, as shown in Table 1.

Table 1
Properties of the vibrator type KELLER L-BETA [24].

Length	3.10 m
Diameter	320 mm
Weight	1815 kg
Power	100 kW
Frequency	60 Hz
Amplitude of horizontal displacement	5 mm
Centrifugal force	201 kN

4. Numerical examples

4.1. Employed model parameters

In all the cases, the soil layer depth is taken as $H = 5$ m, and one single vibrating point at an elevation of $h = H/2$, is considered. The distance between holes, D, has been made variable in the range of 1–4 m. Due to the symmetry of the problem, the spatial domain width is $D/2$.

Three different sandy, quartzitic materials have been modeled, namely [12]:

- CS-0.45: Crystal Silica n^{0}20 sand, with $Dr_0 = 0.45$,
- CS-0.80: Crystal Silica n^{0}20 sand, with $Dr_0 = 0.80$,
- OT-0.77: Ottawa sand with $Dr_0 = 0.77$.

The constitutive model parameters for these soils are listed in Table 2. Fig. 7 shows the sketch of the spatial domain in all the cases, including the location of the vibrating point, while Fig. 8 represents the FE mesh for the particular case of $D/2 = 2$ m.

4.2. Results and discussion

Fig. 9 shows the values of the mean densification function, ϕ_y, for the three soils and for different values of $D/2$, once the treatment has finished (after 10 s of vibration for each one). In all the cases, the trend is the same: the higher the distance between holes, D, the smaller the mean densification, as could be expected. However, the most relevant aspect is the slope of these curves, which is much higher for small values of D, meaning that, for the lower range of distances between holes, a little reduction in D produces an important improvement on the effect of the treatment. On the other hand, for the Crystal Silica sand, for which results for different initial relative densities are obtained (namely CS-0.45 and CS-0.80), the looser the material, the higher the mean densification obtained following the trend experimentally observed in densification laboratory tests [3,4]. This fact indicates, at least in a qualitative way, the correct trend predicted by this numerical model.

Fig. 10 represents the evolution of the densification at points A, B and C (according to Fig. 8) for the Crystal Silica sand with initial relative density of 0.45. Logically, the trend represents an increment of the densification at each point in all the cases, but significantly faster as the point is closer to the point of vibration, as happened with points A and B. The details on this issue are sketched in Fig. 11, where the contour lines represent the amount of densification around the point of vibration at the end of the treatment.

The time of treatment is directly related to the number of holes in a particular zone. For instance, if we want to densify a soil layer of $10,000$ m^2 with a square plant, the horizontal spacing between the holes will determine the number of points to vibrate, and hence, the total time spent on completing the ground improvement. As it was

Table 2
Generalized densification law parameters for the employed sands [12].

Sand	**Crystal Silica n^{0}20-0.45**	**Crystal Silica n^{0}20-0.80**	**Ottawa-0.77**
Abbrev.	CS-0.45	CS-0.80	OT-0.77
Dr_0	0.45	0.80	0.77
e_0	0.817	0.817	0.618
e_{max}	0.97	0.97	0.752
e_{min}	0.63	0.63	0.484
C	2.00	20.00	1.66
Bg	200	200	200
Ct	0.5	0.5	0.5

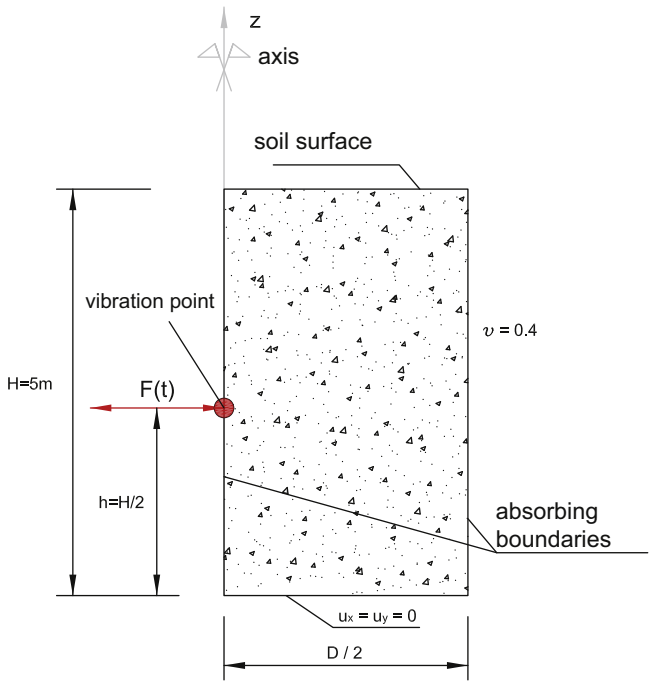

Fig. 7. Spatial domain in the analyzed cases (with different widths).

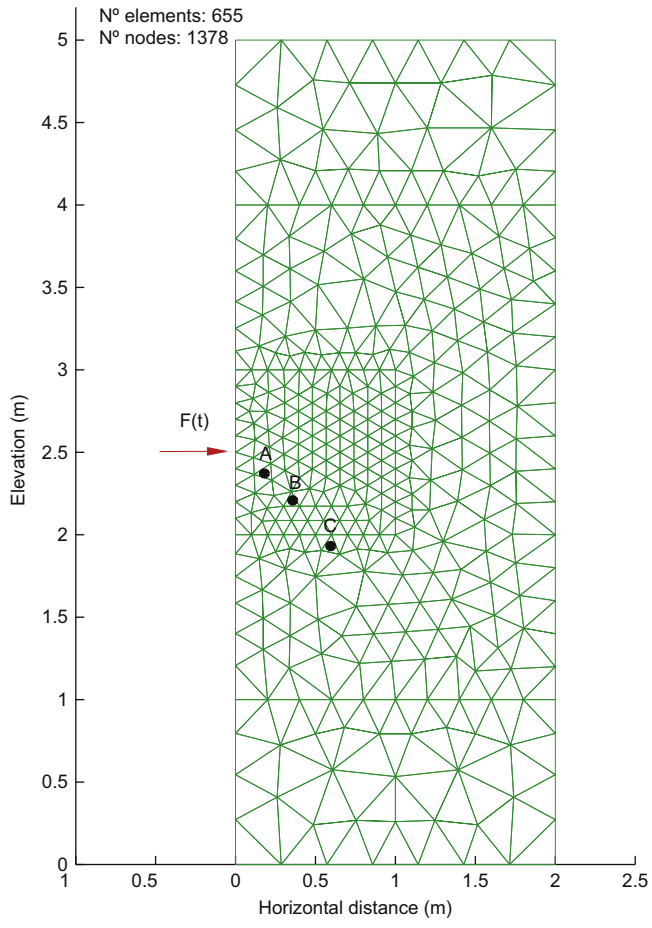

Fig. 8. Mesh for the case $D/2=2.0$ m.

mentioned before, in the simple cases analyzed in this research, there is only one point of vibration in each hole (at the middle of the layer depth), and in each point the vibrator works during 10 s, so the total

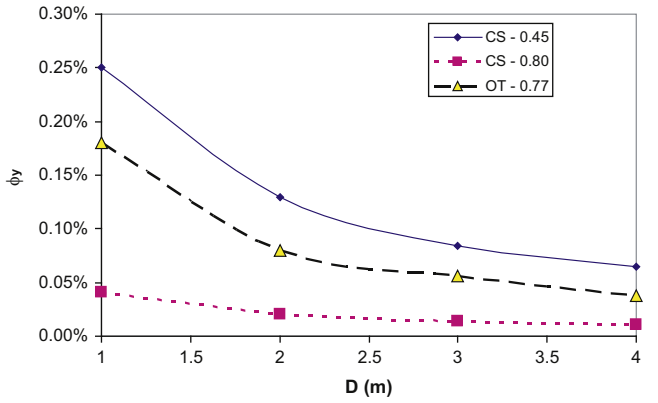

Fig. 9. Evolution of the mean densification function with the distance between holes, D, for the three analyzed soils.

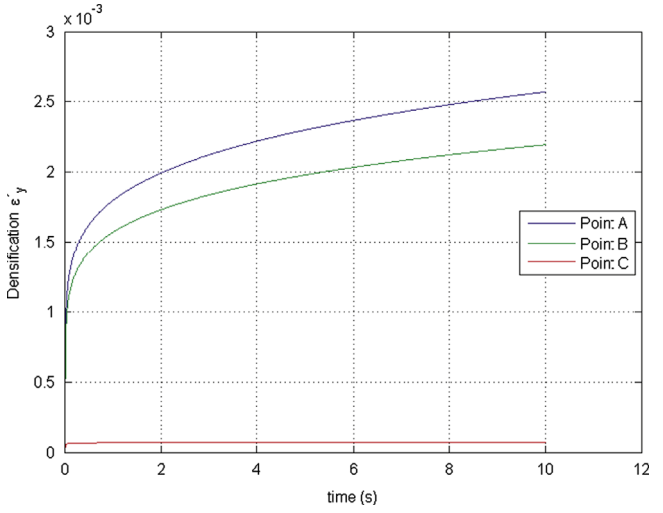

Fig. 10. Evolution of the densification in time of vibration at points A, B and C (see Fig. 8) for CS-0.45 sand.

time of treatment for the analyzed spacing is then calculated in Table 3. By the inspection of this data, the huge difference in time (in other words, in cost) of this technique as a function of the selected separation between holes is self-evident.

Fig. 12 shows the values of the mean densification for the different times of treatment for the three analyzed sands. We can conclude that, the denser the mesh of holes, the more efficient the densification achieved. However, the shapes of the calculated curves show that, for the lower times of treatment, it is worth to increase the number of holes, since the slope is steeper.

As a practical hypothesis of this research, the minimum possible separation between holes which permits this treatment is assumed as $D=1$ m. Hence, the mean densification produced with an influence radius, $D/2$, of 0.5 m. A significant value of 75% of the maximum mean densification is considered herein as a practical final objective of the treatment (called ϕ_{75}). Making the inverse computation, to obtain the maximum possible distance between holes which would achieve ϕ_{75}, it is possible to optimize the spacing between holes. Table 4 shows these optimal results, in terms of total time of treatment, t_{opt}, and hole spacing, D_{opt}, which is in the range of 1.3–1.5 m, for all the studied materials.

It is worth to point out that this is just an example of application of the presented methodology, and hence, these optimal values should not be considered as general recommendations, but quantities which

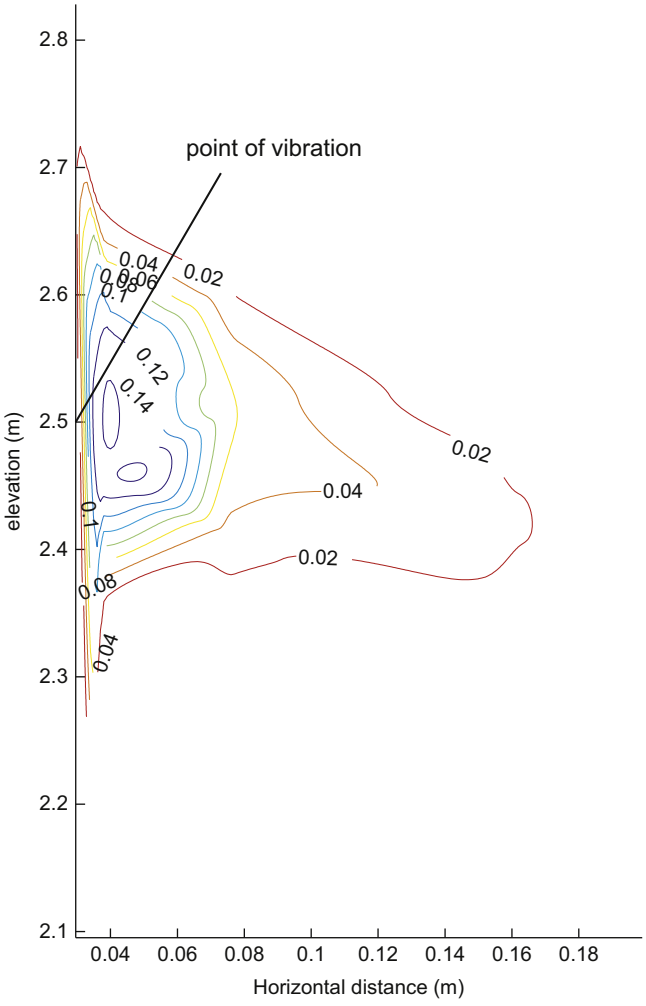

Fig. 11. Details of contour lines of densification around the point of vibration (see Fig. 8) for CS-0.45 sand.

Table 3
Time of treatment at a soil surface of 10,000 m^2. Results for the three analyzed soils, including different values of $D/2$, for soil layer depth $H=5$ m, vibrating during $t=10$ s at each point.

$D/2$ (m)	D (m)	Number of points (N.P.)	Time of treatment		Analyzed sands		
			(s)	(h)	CS-0.45 (ϕ_y)	CS-0.80 (ϕ_y)	OT-0.77 (ϕ_y)
0.5	1	10,000	100,000	28	0.0025	0.000406	0.0018
1	2	2500	25,000	7	0.0013	0.000203	0.000798
1.5	3	1089	10,890	3	0.000845	0.000135	0.000663
2	4	625	6250	2	0.000648	0.000104	0.000383

must be optimized taking into account the precise geometry, soil properties and main vibrating loading features, for each particular problem.

Finally, the mean settlement of the treated soil layer, Δz has also been estimated for all the soils and different values of D. To do that, it is assumed that at each hole, there are five points of vibration. Hence, Δz is equal to the multiplication of the objective mean densification at the end of the treatment, ϕ_y, by the number of points and by the layer elevation, H. Table 5 summarizes these results. For the looser material (CS-0.45), the maximum obtained settlement is 6.25 cm.

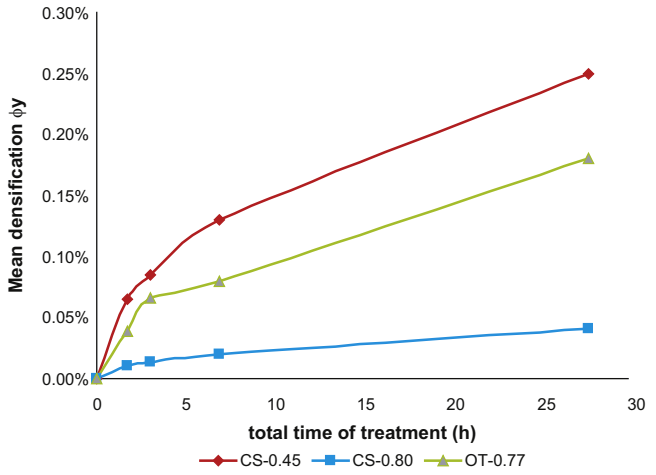

Fig. 12. Evolution of the mean densification with the total time of treatment $D/2=1.5$ m.

Table 4
Optimal results of spacing of holes, for the three studied materials.

CS-0.45			CS-0.80			OT-0.77		
$\phi_{75\%}$	t_{opt} (h)	D_{opt} (m)	$\phi_{75\%}$	t_{opt} (h)	D_{opt} (m)	$\phi_{75\%}$	t_{opt} (h)	D_{opt} (m)
0.19%	17	1.3	0.03%	17.4	1.5	0.14%	18.4	1.4

Table 5
Mean settlements, Δz, at surface after the treatment (5 points of vibration are adopted at each hole).

D (m)	CS-0.45 Δz (cm)	CS-0.80 Δz (cm)	OT-0.77 Δz (cm)
1.0	6.5	1.0	4.5
2.0	3.2	0.5	2.0
3.0	2.1	0.3	1.5
4.0	1.6	0.3	0.9

5. Conclusions

This paper presents a new numerical model as a tool aiding to obtain an optimized design of the vibroflotation soil improvement technique in sandy soils. A Finite Element code, formulated in cylindrical coordinates to represent the axi-symmetry of the problem, includes a Generalized Densification constitutive law, previously used with success to reproduce settlements of sandy soils after earthquakes. For those borders limiting to the surrounding soil, the boundaries have been formulated as absorbing.

The conclusions derived from this research can be summarized as follows:

- The used constitutive law is not only valid for earthquakes, but also for higher frequency loadings, like for instance, the vibrations induced in this particular soil improvement technique. The obtained results are in the range of those observed both in the laboratory and in field cases.
- Horizontal distances between holes of 3–4 m produce very small total densification, which improves significantly as the spacing becomes denser.
- A practical horizontal distance in the range of 1.3–1.5 m has been obtained as optimal to get a value of the 75% of the mean densification in a given sand. For a particular material, it can be concluded that, the denser it is, the higher could be the distance between holes.

Future analyses taking into account deeper layers, more points of vibration in the same hole, and other materials, as well as comparisons with real field data, are required for completing this research, and are currently being developed by the authors.

Acknowledgments

This study has been partially funded by Spanish Ministry of Economy and Competitiveness through the project BIA2012-31678, and the Spanish Ministry of Education through the scholarship FPU12/00684. The financial support to complete this research is gratefully appreciated by the authors.

Appendix A. Elementary FE matrices in axi-symmmetrical problems

Radial (horizontal) and axial (vertical) displacements u, and w are independent on θ. Circular displacement v is null, due to the axisymmetrical nature of the problem.

The relationships between strains and displacements are given by

$$\varepsilon_r = \frac{\partial u}{\partial r}; \quad \varepsilon_z = \frac{\partial w}{\partial z}; \quad \gamma_{rz} = \frac{\partial u}{\partial z} + \frac{\partial w}{\partial r} \tag{28}$$

$$\gamma_{r\theta} = 0; \quad \gamma_{z\theta} = 0 \tag{29}$$

where ε_r, ε_z and γ_{rz} are radial, axial and shear strains respectively.

On the other hand, it is worth to point out that the axial strain causes a horizontal displacements u to those points located at a circumference with radius r, which move until $r+u$. Thus, circumferential strain ε_θ is defined as follows:

$$\varepsilon_\theta = \frac{2\pi(r+u)-2\pi r}{2\pi r} = \frac{u}{r} \tag{30}$$

Hence, in axisymmetric problems, the strains are obtained as

$$\{\varepsilon\} = \begin{pmatrix} \varepsilon_r \\ \varepsilon_z \\ \varepsilon_\theta \\ \gamma_{rz} \end{pmatrix} = \begin{pmatrix} \frac{\partial u}{\partial r} \\ \frac{\partial w}{\partial z} \\ \frac{u}{r} \\ \frac{\partial u}{\partial z} + \frac{\partial w}{\partial r} \end{pmatrix} \tag{31}$$

In finite elements, local areal coordinates are used. These coordinates are defined as [26]:

$$L_i = \frac{a_i + b_i \cdot r + c_i \cdot z}{2A} \tag{32}$$

where coefficients a_i, b_i, c_i are

$$\begin{aligned} &a_1 = r_2 z_3 - r_3 z_2; \quad b_1 = z_2 - z_3; \quad c_1 = r_3 - r_2; \\ &a_2 = r_3 z_1 - r_1 z_3; \quad b_2 = z_3 - z_1; \quad c_2 = r_1 - r_3; \\ &a_3 = r_1 z_2 - r_2 z_1; \quad b_3 = z_1 - z_2; \quad c_1 = r_2 - r_1. \end{aligned} \tag{33}$$

Elastic stress–strain relationship is given by $\mathbf{D}^e$:

$$[\mathbf{D}]^e = \begin{pmatrix} D_1 & D_2 & D_2 & 0 \\ D_2 & D_1 & D_2 & 0 \\ D_2 & D_2 & D_1 & 0 \\ 0 & 0 & 0 & D_3 \end{pmatrix} \tag{34}$$

$$D_1 = \lambda \cdot \frac{1-\nu}{\nu}; \quad D_2 = \lambda; \quad D_3 = G; \quad \lambda = \frac{2G\nu}{1-2\nu} \tag{35}$$

where G denotes the soil shear elastic modulus, ν is de Poisson's ratio, and λ is Lamé's coefficient.

For quadratic, triangular finite elements (6 nodes), the formulation, according to [27], is

Shape functions: Nodes i, j, k denote corner, and l, m, n represent those nodes located at the middle of each side. Areal coordinates, L_1, L_2, L_3, L_4, L_5, L_6 (according to (32)) and (33) are given by

$$\begin{aligned} &N_i^e(r,z) = N_1^e(r,z) = L_1(2L_1-1); \quad N_l^e(r,z) = N_4^e(r,z) = 4L_1L_2 \\ &N_j^e(r,z) = N_2^e(r,z) = L_2(2L_2-1); \quad N_m^e(r,z) = N_5^e(r,z) = 4L_2L_3 \\ &N_k^e(r,z) = N_3^e(r,z) = L_3(2L_3-1); \quad N_n^e(r,z) = N_6^e(r,z) = 4L_1L_3 \end{aligned} \tag{36}$$

Hence, shape functions are

$$[N] = \begin{bmatrix} N_1^e & 0 & N_2^e & 0 & N_3^e & 0 & N_4^e & 0 & N_5^e & 0 & N_6^e & 0 \\ 0 & N_1^e & 0 & N_2^e & 0 & N_3^e & 0 & N_4^e & 0 & N_5^e & 0 & N_6^e \end{bmatrix} \tag{37}$$

To obtain the elementary stiffness matrix, $[K]^e$, it is necessary previously computing $[B]$ given by

$$[B] = \begin{bmatrix} \frac{\partial}{\partial r} & 0 \\ 0 & \frac{\partial}{\partial z} \\ \frac{1}{r} & o \\ \frac{\partial}{\partial z} & \frac{\partial}{\partial r} \end{bmatrix} \cdot [N] \tag{38}$$

Finally, the elementary matrices are

Stiffness matrix $[\mathbf{K}]^e$:

$$[\mathbf{K}]^e = \int_\Omega \frac{\partial [N]^T}{\partial l} \cdot [\mathbf{D}]^e \cdot \frac{\partial [N]}{\partial m} \, d\Omega = 2\pi \int_A [B]^T \cdot [\mathbf{D}]^e \cdot [B] \cdot r \, dA \tag{39}$$

where ∂l, ∂m denote ∂r, ∂z or:

$$[\mathbf{K}]^e = 2\pi \int_A [B]^T \cdot [\mathbf{D}]^e \cdot [B] \cdot r_{gc} \cdot 2A \, dr \, dz \tag{40}$$

where A represents the element area, and r_{gc} is the radial coordinate of the element gravity centre.

Mass matrix $[\mathbf{M}]^e$:

$$[M]^e = \int_A [N]^T \cdot \rho \cdot [N] \, dA = 2\pi\rho \int_A [N]^T \cdot [N] \cdot r_{gc} \cdot 2A \, dr \, dz \tag{41}$$

,

Mass force vector $\{f_g\}^e$:

$$\{f_m\}^e = \int_A [N]^T \cdot \rho \, dA = 2\pi \int_A [N]^T \cdot \rho \cdot r \, dr \, dz \tag{42}$$

or:

$$\{f_m\}^e = 2\pi \int_A [N]^T \cdot \{\rho\} \cdot r_{gc} \cdot 2A \, dr \, dz \tag{43}$$

Finally, $\{f_g\}^e$ is obtained as follows:

$$\{f_g\}^e = \{f_m\}^e \cdot \{a_g\} \tag{44}$$

where $\{a_g\}$ denotes the vector of gravitational accelerations in axisymmetric reference system.

References

[1] Mitchell J. In-place treatment of foundation soils. J Soils Mech Found Div ASCE 1970;96(SM1):73–110.
[2] Brown R. Vibroflotation compaction of cohesionless soils. J Geotech Eng Div ASCE 1977;103(GT12):1437–51.
[3] Silver M, Seed H. Changes in sand during cyclic loadings. J Soil Mech Found Div ASCE 1971(97):1171–82.
[4] Seed H, Silver M. Settlement of dry sands during earthquakes. J Soil Mech Found Div ASCE 1972(98):381–96.
[5] Finn WDL, Seed HB, Martin GR. Fundamentals of liquefaction under cyclic loading. J Geotech Eng Div 1975;101(GT5):423–38.
[6] Bement RAP, Selby AR. Compaction of granular soils by uniform vibration equivalent to vibrodriving of piles. Geotech Geol Eng 1997;15:121–43.
[7] Arnold M, Herle I. Comparison of vibrocompaction methods by numerical simulations. Int J Numer Anal Methods Geomech 2009;33(16):1823–38.
[8] von Wolffersdorff P. A hypoplastic relation for granular materials with a predefined limit state surface. Mech Cohesive-Frict Mater 1996;1(4):251–71.
[9] Niemunis A, Herle I. Hypoplastic model for cohesionless soils with elastic strain range. Mech Cohesive-Frict Mater 1997;2(4):279–99.
[10] Cuéllar V. Rearrangement measure theory applied to dynamic behavior of sand [Ph.D. dissertation]. Evanston, Illinois: Northwestern University; August 1974.

[11] Cuéllar V. Simple shear theory for the one-dimensional behavior of dry sand under cyclic loading. In: Proceedings of international symposium on dynamical methods in soil and rock mechanics, Karlsruhe, West Germany; 1977.
[12] Blazquez R, López-Querol S. Generalized densification law for dry sand subjected to dynamic loading. Soil Dyn Earthq Eng 2006;26(9):888–98.
[13] Ko H, Scott R. Deformation of sand in hydrostatic compression. J Soil Mech Found Div ASCE 1967(93):137–56.
[14] Zienkiewicz O, Chang C, Hilton E. Non-linear seismic response and liquefaction. Int J Numer Anal Methods Geomech 1978(2):381–404.
[15] Papadimitriou AG, Bouckovalas GD, Dafalias YF. Plasticity model for sand under small and large cyclic strains. J Geotech Geoenviron Eng 2001;127(11):973–83.
[16] López-Querol S, Blazquez R. Validation of a new endochronic liquefaction model for granular soil by using centrifuge test data. Soil Dyn Earthq Eng 2007;27(10):920–37.
[17] López-Querol S, Blazquez R. Liquefaction and cyclic mobility model for saturated granular media. Int J Numer Anal Methods Geomech 2006;30(5):413–39.
[18] Oñate E. Cálculo de Estructuras por el Método de Elementos Finitos, Centro Internacional de Métodos Numéricos en Ingeniería, Barcelona, Spain; 1992 [in Spanish].
[19] Newmark N. A method of computation for structural dynamic. J Eng Mech Div ASCE 1959;85:67–94.
[20] Zienkiewicz O, Chan A, Pastor M, Schrefler B, Shiomi T. Computational geomechanics. UK: John Wiley; 1999.
[21] Lysmer J, Kuhlemeyer R. Finite dynamic model for infinite media. J Eng Mech Div ASCE 1969;95(4):859–77.
[22] Toshinawa T, Ohmachi T. Ground motion simulation by using simplified three-dimensional finite element method. In: Proceedings of 10th world conference on earthquake engineering. Netherlands: Balkema-Rotterdam; 1992. p. 851–6.
[23] Verruijt A. Soil dynamics. Delft, Netherlands: Delft University of Technology; 2005.
[24] Torres García-Lomas E, Candela González J. Tratamientos de mejora del terreno. Vibroflotación. Columnas de grava. Caso de obra: Enlace M-50 con la M-511 en Boadilla del Monte, Madrid, KELLERTERRA, Spain; 2008 [in Spanish].
[25] Hamming R. Digital filters. City Englewood Cliffs: Prentice Hall; 1977.
[26] Zienkiewicz O, Taylor R. El Método de los Elementos Finitos. Formulación básica y Problemas Lineales, vol. 1. Madrid, Spain: McGraw-Hill; 1994.
[27] Chaves E, Mínguez R. Mecánica Computacional en la Ingeniería con Aplicaciones en Matlab, UCLM, Ciudad Real, Spain; 2010.